Kinetic Analysis of the Stepwise Formation of a Long-Range DNA Interstrand Cross-link by a Dinuclear Platinum Antitumor Complex: Evidence for Aquated Intermediates and Formation of Both Kinetically and Thermodynamically Controlled Conformers

John W. Cox,[†] Susan J. Berners-Price,*[,‡] Murray S. Davies,[‡] Yun Qu,[†] and Nicholas Farrell*[,†]

Contribution from the School of Science, Griffith University, Nathan, Brisbane, Queensland 4111, Australia, and Department of Chemistry, Virginia Commonwealth University, Richmond, Virginia 23284-2006

Received April 12, 2000. Revised Manuscript Received December 26, 2000

Abstract: Reported here is a detailed study of the kinetics and mechanism of formation of a 1,4 GG interstrand cross-link by $[\{trans\text{-}PtCl(NH_3)_2\}_2(\mu\text{-}NH_2(CH_2)_nNH_2)]^{2+}$ (1,1/t,t ($n = 6$), **1**), the prototype of a novel class of platinum antitumor complexes. The reaction of the self-complementary 12-mer duplex 5′-{d(ATAT**G**TA-CATAT)$_2$} with ^{15}N-**1** has been studied at 298 K, pH 5.4, by [^{1}H,^{15}N] HSQC 2D NMR spectroscopy. Initial electrostatic interactions with the duplex are observed for **1** and the monoaqua monochloro species (**2**). Aquation of **1** to yield **2** occurs with a pseudo-first-order rate constant of $(4.15 \pm 0.04) \times 10^{-5}$ s^{-1}. **2** then undergoes monofunctional binding to the guanine N7 of the duplex to form **3** (G/Cl) with a rate constant of 0.47 ± 0.06 M^{-1} s^{-1}. There is an electrostatic interaction between the unbound {PtN$_3$Cl} group of **3** and the duplex, which is consistent with H-bonding interactions observed in the molecular model of the monofunctional (G/Cl) adduct. Closure of **3** to form the 1,4 GG interstrand cross-link (**5**) most likely proceeds via the aquated (G/H$_2$O) intermediate (**4**) (pseudo-first-order rate constant = $(3.62 \pm 0.04) \times 10^{-5}$ s^{-1}) followed by closure of **4** to form **5** (rate constant = $(2.7 \pm 1.5) \times 10^{-3}$ s^{-1}). When closure is treated as direct from **3** (G/Cl) the rate constant is $(3.39 \pm 0.04) \times 10^{-5}$ s^{-1}. Closure is ca. 10−55-fold faster than that found for 1,2 GG intrastrand cross-link formation by the diaqua form of cisplatin. Changes in the ^{1}H and ^{15}N shifts of the interstrand cross-link **5** indicate that the initially formed conformer (**5(i)**) converts irreversibly into other product conformer(s) **5(f)**. The NMR data for **5(i)** are consistent with a molecular model of the 1,4 GG interstrand cross-link on B-form DNA, which shows that the NH$_2$ protons have no contacts except with solvent. The NMR data for **5(f)** show several distinct NH$_2$ environments indicative of interactions between the NH$_2$ protons and the DNA. HPLC characterization of the final product showed only one major product peak that was confirmed by ESI-FTICR mass spectroscopy to be a cross-linked adduct of ^{15}N-**1** and the duplex. The potential significance of these findings to the antitumor activity of dinuclear platinum complexes is discussed.

Introduction

Multinuclear platinum compounds comprising di- or trinuclear platinum centers linked by variable length diamine chains constitute a new and discrete class of platinum-based anticancer agents.[1] One example of this series, the trinuclear $[(trans\text{-}PtCl(NH_3)_2)_2\{\mu\text{-}trans\text{-}Pt(NH_3)_2(NH_2(CH_2)_nNH_2)_2\}]^{4+}$ (1,0,1/t,t,t ($n = 6$) or BBR3464), is the first genuinely "nonclassical" platinum derivative to enter clinical trials. After a highly promising Phase I trial indicated responses in colon and pancreatic cancers,[2] this drug has now advanced to Phase II clinical trials. The compounds of this class exhibit significantly enhanced antitumor activity relative to cisplatin and its derivatives.[1,2] Development of these compounds was driven by the hypothesis that complexes with distinctly different DNA binding mechanisms may exhibit unique biological activity in comparison to the current mononuclear clinically used agents.[1,3]

Di- and tri-nuclear compounds exemplified by the structures below represent only one structurally distinct subclass of polynuclear platinum compounds—they are bifunctional platinating agents because only two Pt−Cl bonds are present. Their intrinsic differences are dictated by the separation between the two platinating centers and the overall charge on the molecule, caused by the presence of the extra "noncoordinating" tetraamineplatinum moiety.[1] Both of these structures present similar *profiles* of biological activity that differ significantly from that of cisplatin. The trinuclear compound is more potent than its dinuclear analogue (and significantly more so than cisplatin) and may be attributed to a combination of enhanced cellular uptake and enhanced target (DNA) affinity.[4]

* Address correspondence to this author.
[†] Virginia Commonwealth University.
[‡] Griffith University.

(1) Farrell, N.; Qu, Y.; Bierbach, U.; Valsecchi, M.; Menta, E. In *Cisplatin: Chemistry and Biochemistry of a Leading Anticancer Drug*; Lippert, B., Ed.; Wiley VCH: New York, 1999; pp 479−496.

(2) Calvert, P. M.; Highley, M. S.; Hughes, A. N.; Plummer, E. R.; Azzabi, A. S. T.; Verrill, M. W.; Camboni, M. G.; Verdi, E.; Bernareggi, A.; Zucchetti, M.; Robinson, A. M.; Carmichael, J.; Calvert, A. H. In *AACR-NCI-EORTC International Conference, Molecular Targets and Cancer Therapeutics*: Washington, 1999; Abstract 333.

(3) Farrell, N. *Comments Inorg. Chem.* **1995**, *16*, 373−389.

(4) Roberts, J. D.; Peroutka, J.; Farrell, N. *J. Inorg. Biochem.* **1999**, *77*, 51−57.

10.1021/ja0012772 CCC: $20.00
Published on Web 01/25/2001

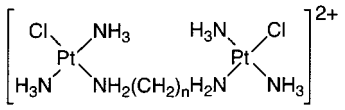

1,1/t,t (n = 6)

1

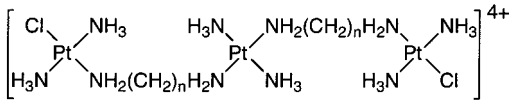

1,0,1/t,t,t (n = 6)

BBR3464

Several aspects of the DNA binding profiles for these compounds are notably different from those found for cisplatin and other mononuclear platinum(II) compounds. First, these compounds are capable of forming bifunctional DNA adducts structurally distinct from those formed by cisplatin, especially long-range (Pt, Pt) interstrand cross-links.[1,5] These cross-links represent a new class of DNA adducts of anticancer agents; situated in the major groove by virtue of guanine N7 binding, the structures will be different not only from those of cisplatin, but also from long-range minor groove cross-linking agents such as CC1065 and Bizelesin. The flexibility of the bridging group allows for the formation of a number of different cross-links, while classically bifunctional mononuclear compounds are restricted in the number and type of cross-links they can form.[1,7,8] Depending on sequence, both A- and Z-form DNA are induced by binding to DNA of polynuclear platinum compounds.[9] Further, 1,3- and 1,4-(Pt, Pt)-interstrand cross-links formed by 1,1/t,t compounds do not significantly bend DNA and thus are not recognized efficiently by HMG1 proteins.[10] Such protein recognition is postulated to be an important aspect of the antitumor activity of cisplatin[11−13] and lends support to our stated hypothesis that structurally unique DNA adduct structures may lead to different "downstream" effects which may result in a significantly different profile of antitumor activity.[3]

To delineate the differences between the antitumor activity of mononuclear complexes, as represented by cisplatin on one hand and the polynuclear platinum complexes on the other, it is important to understand the kinetic and structural aspects of the DNA binding of the new agents. [^{1}H,^{15}N] HSQC NMR has proven to be a powerful method for studying DNA platination reactions by cisplatin and other mononuclear platinum complexes.[14−19] The technique requires the use of ^{15}N-labeled compounds and allows observation of all platinated species at low (micromolar) concentrations. The spectra are simplified because only ^{1}H and ^{15}N resonances derived from platinum am(m)ine species are seen and the ^{15}N shifts are strongly influenced by the trans ligand.[20,21] [^{1}H,^{15}N] HSQC NMR is especially useful for following the reactions of the di- and trinuclear platinum am(m)ine complexes because ^{15}N-labeling of both $^{15}NH_2$ and $^{15}NH_3$ groups is possible.[22] Although this gives rise to spectra that are more complex than those observed for cisplatin, it proves advantageous because the NH_2 and NH_3 regions of the [^{1}H,^{15}N] 2D NMR spectra are well separated and the reaction can be followed independently in each region.

In this contribution we discuss the kinetics of interstrand cross-link formation by the dinuclear platinum compound [{*trans*-PtCl(NH_3)$_2$}$_2$(μ-$NH_2(CH_2)_nNH_2$)]$^{2+}$ (**1**), 1,1/t,t ($n = 6$), the prototype for this class of multinuclear platinum complexes. [^{1}H,^{15}N] HSQC NMR was used to examine the DNA binding kinetics of ^{15}N-**1** and the self-complementary 12-mer duplex 5′-{d(ATATGTACATAT)$_2$} (**I**). A 1,4 interstrand cross-link is formed through binding to the GN7 site of each strand:

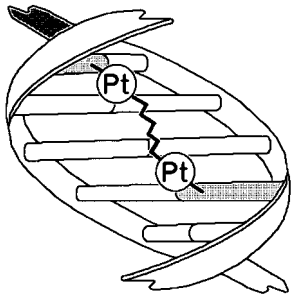

Molecular models of the monofunctional and bifunctional adducts on B-form DNA were also constructed to examine the environment of the am(m)ine ligands of **1**, specifically their close contacts (hydrogen bonds) with duplex **I**.

Experimental Section

Chemicals. The sodium salt of the HPLC purified oligonucleotide 5′-d(ATATGTACATAT)-3′ (**I**) was purchased from OSWEL. The nitrate salt of fully ^{15}N-labeled [{*trans*-PtCl($^{15}NH_3$)$_2$}$_2$(μ-$H_2{}^{15}$N-

Scheme 1

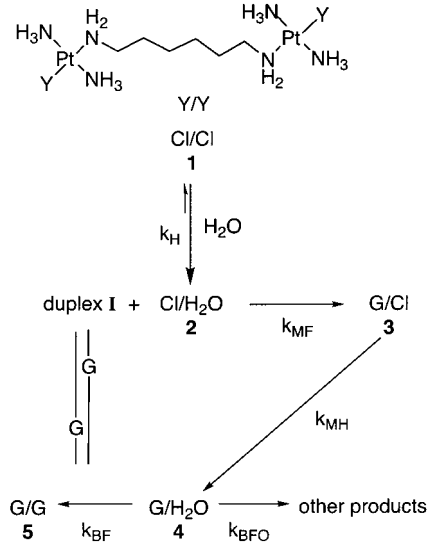

(5) Zaludová, R.; Zakovská, A.; Kašparková, J.; Balcarová, Z.; Kleinwächter, V.; Vrána, O.; Farrell, N.; Brabec, V. *Eur. J. Biochem.* **1997**, *246*, 508−517.
(6) Rajski, S. R.; Williams, R. M. *Chem. Rev.* **1998**, *98*, 2723−2796.
(7) Kašparková, J.; Mellish, K. J.; Qu, Y.; Brabec, V.; Farrell, N. *Biochemistry* **1996**, *35*, 16705−16713.
(8) Brabec, V.; Kašparková, J.; Vrána, O.; Nováková, O.; Cox, J. W.; Qu, Y.; Farrell, N. *Biochemistry* **1999**, *38*, 6781−6790.
(9) McGregor, T. D.; Balcarová, Z.; Qu, Y.; Tran, M.-C.; Zaludová, R.; Brabec, V.; Farrell, N. *J. Inorg. Biochem.* **1999**, *77*, 43−46.
(10) Kašparková, J.; Farrell, N.; Brabec, V. *J. Biol. Chem.* **2000**, *275*, 15789−15798.
(11) Ohndorf, U.-M.; Rould, M. A.; He, Q.; Pabo, C. O.; Lippard, S. J. *Nature* **1999**, *399*, 708−712.
(12) Ohndorf, U. M.; Whitehead, J. P.; Raju, N. L.; Lippard, S. J. *Biochemistry* **1997**, *36*, 14807−14815.
(13) Jamieson, E. R.; Lippard, S. J. *Chem. Rev.* **1999**, *99*, 2467−2498.
(14) Barnham, K. J.; Berners-Price, S. J.; Frenkiel, T. A.; Sadler, P. J. *Angew. Chem., Int. Ed.* **1995**, *34*, 1874−1877.
(15) Berners-Price, S. J.; Barnham, K. J.; Frey, U.; Sadler, P. J. *Chem. Eur. J.* **1996**, *2*, 1283−1291.
(16) Reeder, F.; Guo, Z.; Murdoch, P. del S.; Corazza, A.; Hambley, T. W.; Berners-Price, S. J.; Chottard, J. C.; Sadler, P. J. *Eur. J. Biochem.* **1997**, *249*, 370−382.
(17) Davies, M. S.; Berners-Price, S. J.; Hambley, T. W. *J. Am. Chem. Soc.* **1998**, *120*, 11380−11390.

$(CH_2)_n{}^{15}NH_2)]^{2+}$ (1,1/t,t ($n = 6$); ^{15}N-**1**) was prepared by an adaptation of previously described 1,1/t,t synthesis, using the appropriately labeled ligands.[22]

Sample Preparation. A stock solution of 5′-d(ATATGTACATAT)-3′ (**I**) was prepared in 500 μL of 5% D_2O in H_2O. The concentration was estimated spectrophotometrically to be 23.1 mM[23,24] by using the absorption coefficient provided by OSWEL ($\epsilon_{260} = 126 \times 10^3$ M^{-1} cm^{-1}).

Reaction of Duplex I with ^{15}N-1. I stock solution (75.9 μL, 8.8×10^{-7} mol of duplex), sodium phosphate solution (30 μL, 200 mM, pH 5.2), TSP (sodium 3-trimethylsilyl-D_4-propionate) (2 μL of 13.3 mM), and 5% D_2O in H_2O (272.1 μL) were combined, and the pH was adjusted to pH 5.4 by addition of $HClO_4$ (0.2 M, 2 μL). A total of 10 μL of the solution was removed for pH measurement. This produced a reaction mixture volume of 372 μL and contained 8.6×10^{-7} mol of duplex.[23] A melting profile was performed on the unplatinated duplex by obtaining ^{1}H spectra at 5 K increments between 288 and 318 K. After slowly cooling the mixture to 298 K a 20 μL aliquot of a freshly prepared solution of ^{15}N-**1** (1.05 mg, 1.35 μmol) in 5% D_2O in H_2O (42.3 μL) was then added to give final concentrations of **I** (duplex), 2.3 mM,[23] phosphate buffer, 15 mM, and ^{15}N-**1**, 1.63 mM. The reaction at 298 K was followed by ^{1}H and [^{1}H,^{15}N] NMR for a total of 61 h.

Instrumentation. The NMR spectra were recorded on a Varian UNITY-INOVA 600 MHz spectrometer (^{1}H, 599.92 MHz; ^{15}N, 60.79 MHz). The ^{1}H NMR chemical shifts are internally referenced to TSP and the ^{15}N chemical shifts externally referenced to $^{15}NH_4Cl$ (1.0 M in 1.0 M HCl in 5% D_2O in H_2O). The ^{1}H spectra were acquired with water suppression using the WATERGATE sequence.[25] The two-dimensional [^{1}H,^{15}N] heteronuclear single-quantum coherence (HSQC) NMR spectra (decoupled by irradiation with the GARP-1 sequence during the acquisition) were recorded by using the sequence of Stonehouse et al.,[26] as described previously.[17] Samples were not spun during the acquisition of data. All samples (including buffers, acids, etc.) were prepared so that there was a 5% D_2O/95% H_2O concentration (for deuterium lock but with minimal loss of signal as a result of deuterium exchange). Spectra were recorded at 298 K, and the sample was maintained at this temperature when not immersed in the NMR probe.

Typically for 1D ^{1}H spectra, 64 or 128 transients were acquired with use of a spectral width of 12 kHz and a relaxation delay of 1.5 s. For kinetics studies involving [^{1}H,^{15}N] HSQC NMR spectra, 4 or 8 transients were collected for 128−160 increments of t_1 (allowing spectra to be recorded on a suitable time scale for the observed reaction), with an acquisition time of 0.152 s and spectral widths of 4 kHz in f_2 (^{1}H) and 1.8 kHz in f_1 (^{15}N). 2D spectra were completed in 14−36 min. The 2D spectra were processed using Gaussian weighting functions in both dimensions, and zero-filling by ×2 in the f_1 dimension. The pH of the solutions was measured on a Shindengen pH Boy-P2 (su19A) pH meter and calibrated against pH buffers of pH 6.9 and 4.0. The volume of 5.0 μL of the solution was placed on the electrode surface and the pH recorded. These aliquots were not returned to the bulk solution (as the electrode leaches Cl^-). Adjustments in pH were made with 0.04, 0.2, and 1.0 M $HClO_4$ in 5% D_2O in H_2O, or 0.04, 0.2, and 1.0 M NaOH in 5% D_2O in H_2O.

Data Analysis. The kinetic analysis of the reaction was undertaken by measuring peak volumes in the Pt-NH_3 regions of the [^{1}H,^{15}N] spectra using the Varian VNMR software package and calculating the relative concentrations of the various {Pt_2} species at each time point, in a manner similar to that described previously for reactions with cisplatin.[15,17] Peak volumes were determined by using an identical vertical scale and threshold value in successive spectra. ^{195}Pt satellites were not resolved for any of the peaks, presumably a result of relaxation through chemical shift anisotropy.[27] All species, other than ^{15}N-**1**, gave rise to two NH_3 peaks for the nonequivalent {PtN_3Y} groups. In some cases, overlap between peaks was significant (e.g., the peak for the nonaquated {PtN_3Cl} group of the monoaqua monochloro species (**2**) is coincident with the peak for **1**[22]), but in these instances, it was only one of the pair of peaks that was overlapped. Thus, reliable intensities were obtained by doubling the volume of the second (discrete) peak. Most species also gave rise to resolved peaks in the Pt-NH_2 region of the [^{1}H,^{15}N] spectra and comparison of the time-dependent changes in the two regions was used to confirm the peak assignments.

The appropriate differential equations were integrated numerically, and rate constants were determined by a nonlinear optimization procedure with the program SCIENTIST (Version 2.01, MicroMath, Inc.). The errors represent one standard deviation. In all cases the data were fit by using appropriate first- and second-order rate equations. Minima were found by using simulations, and by gradually optimizing the input parameters, fixing some while others were refined, then finally allowing all parameters to be refined simultaneously. The kinetic models used are discussed below and are provided as Supporting Information.

HPLC Analyses. The HPLC analyses were performed on a JASCO high-performance liquid chromatograph with MD910 multiwavelength detector, on a μBondapak C_{18} reverse phase column, using a binary gradient with an aqueous $CH_3CO_2NH_4$ solution (50 mM) as eluant A and CH_3CN as eluant B. The major adduct was collected by using a preparative column under the same eluant conditions. The collected solution was evaporated to ∼0.5 mL at room temperature and ethanol precipitated. The precipitate was dissolved in 1 mL of water and lyophilized to yield 0.6 mg of cross-linked duplex. Electrospray ionization Fourier transform ion cyclotron resonance mass spectrometry was used to determine the binding mode for the duplex [d(ATATG-TACATAT)$_2$-[{*trans*-Pt($^{15}NH_3$)$_2$}$_2$(μ-$^{15}NH_2(CH_2)_6{}^{15}NH_2$)]] (Calcd 7863.78 amu). The ESI-FTICR mass spectrum was consistent with the bifunctional adduct (refer to Supporting Information).

Molecular Modeling. Molecular models of monofunctional and bifunctional adducts of **1** bound to the DNA duplex 5'-{d(ATAT**G**-TACATAT)$_2$} were generated, as described previously.[8] The computations were performed with the program HyperChem (HyperCube, Inc., Ontario, Canada; Molecular Simulations, Inc., San Diego, CA.) with a derivative of the AMBER parameter set and all-atom force field DNA/Pt, developed by Yao et al.[28,29] DNA helical distortions (the base step parameters tilt, twist, and roll, and the base pair parameters buckle, opening, and propeller twist) were calculated with the program NAMOT (available from the Los Alamos National Laboratory, http://www.t10.lanl.gov/namot/). The distance-dependent dielectric constant of $\epsilon = 4r_{ij}$ commonly used for calculations of DNA was applied to account for solvent effects and the electrostatic and van der Waals terms were each scaled by 0.5, which is common practice for calculations involving DNA.[30] Further details of the molecular modeling methodology can be found in the Supporting Information.

Results

The preparation of fully ^{15}N-labeled [{*trans*-PtCl($^{15}NH_3$)$_2$}$_2$-(μ-$^{15}NH_2(CH_2)_6{}^{15}NH_2$)]$^{2+}$ (^{15}N-**1**) and the characterization of **1**

(18) Murdoch, P. del S.; Guo, Z.; Parkinson, J. A.; Sadler, P. J. *J. Biol. Inorg. Chem.* **1999**, *4*, 32−38.

(19) Chen, Y.; Parkinson, J. A.; Guo, Z.; Brown, T.; Sadler, P. J. *Angew. Chem.* **1999**, *111*, 2192−2196; *Angew. Chem., Int. Ed.* **1999**, *2138*, 2060−2063.

(20) Appleton, T. G.; Hall, J. R.; Ralph, S. F. *Inorg. Chem.* **1985**, *24*, 4685−4693.

(21) Berners-Price, S. J.; Sadler, P. J. *Coord. Chem. Rev.* **1996**, *151*, 1−40.

(22) Davies, M. S.; Cox, J. W.; Berners-Price, S. J.; Barklage, W.; Qu, F.; Farrell, N. *Inorg. Chem.* **2000**, *39*, 1710−1715.

(23) Both the ^{1}H NMR spectrum and HPLC analysis of the final product showed a large excess of unplatinated duplex indicating that the calculated concentration of the stock solution was underestimated significantly. For the purposes of the kinetic fit we assumed a duplex concentration of 2.93 mM. This was derived from a recalculated stock solution concentration of 31.2 mM which was obtained using an absorption coefficient ϵ_{260} =186350 M^{-1} cm^{-1} for (duplex) **I**, derived from the data in ref.24.

(24) Kallansrud, G.; Ward, B. *Anal. Biochem.* **1996**, *236*, 134−138.

(25) Piotto, M.; Saudek, V.; Sklenar, V. *J. Biomol. NMR* **1992**, *2*, 661−665.

(26) Stonehouse, J.; Shaw, G. L.; Keeler, J.; Laue, E. D. *J. Magn. Reson. Ser. A* **1994**, *107*, 174−184.

(27) Ismail, I. M.; Kerrison, S. J. S.; Sadler, P. J. *Polyhedron* **1982**, *1*, 57−59.

(28) *HyperChem Computational Chemistry*; HyperChem, Release 4.5; HyperCube, Inc.: Ontario, Canada, 1995; pp 142−144 and 151−152.

(29) Yao, S.; Plastaras, J. P.; Marzilli, L. G. *Inorg. Chem.* **1994**, *33*, 1−6077.

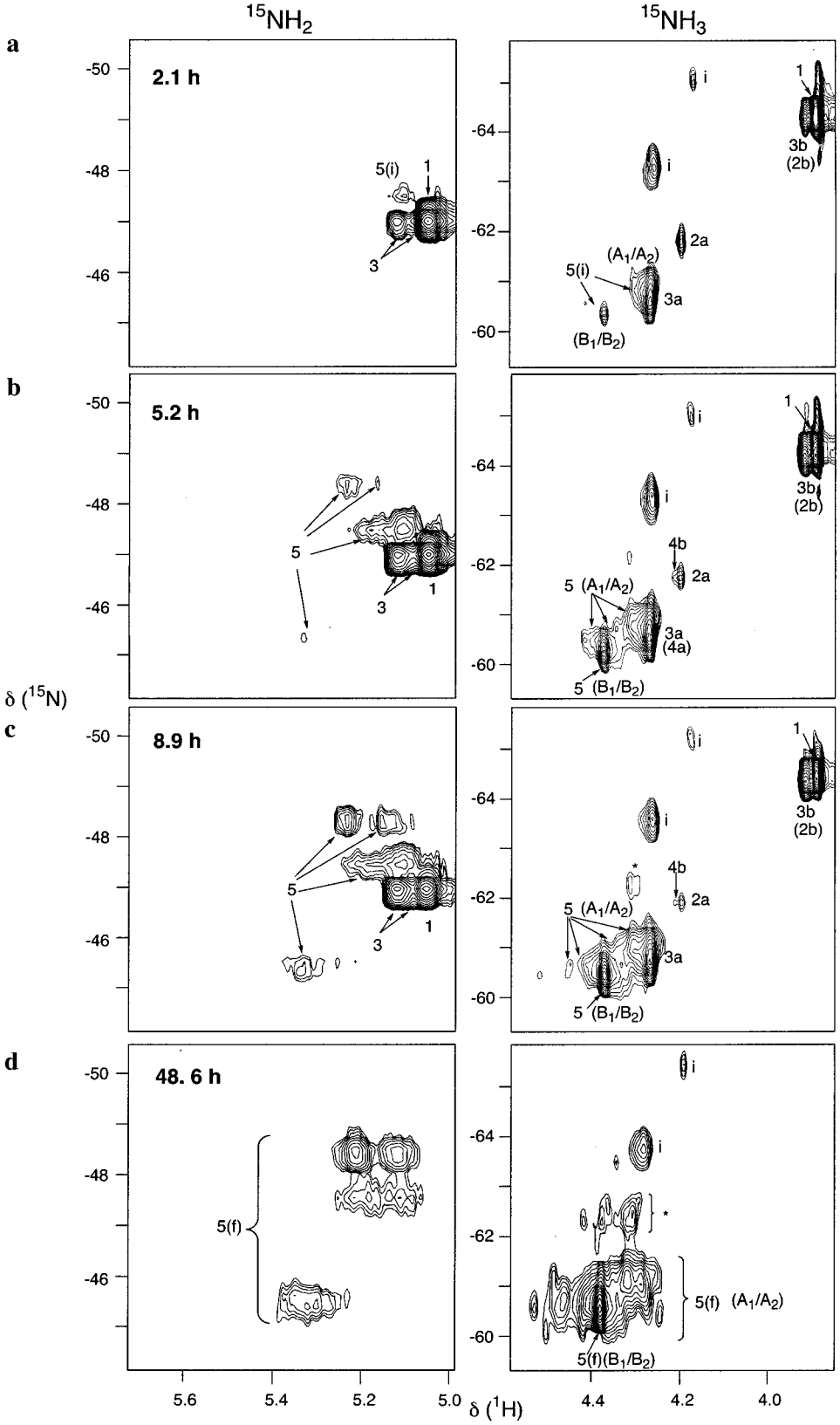

Figure 1. 2D [^{1}H,^{15}N] HSQC NMR (600 MHz) spectra at 298 K of duplex **I** after reaction with ^{15}N-**1** for (a) 2.1, (b) 5.2, (c) 8.9, and (d) 48.6 h. Peaks are assigned to the NH_3 and NH_2 groups in structures **1**−**5** (see Scheme 1 and Table 1). Peaks labeled i are due to minor impurities in the sample of ^{15}N-**1** (see Supporting Information). For the bifunctional adduct (**5**) the assignments A_1/A_2 and B_1/B_2 correspond to the different NH_3 environments observed in the model (Figure 5) which are H-bonded to O6 of the bases (B) and located close to the phosphate backbone (A). The initial adduct (**5(i)**) transforms into other thermodynamically preferred final adduct conformers (**5(f)**). Peaks labeled with an asterisk in the NH_3 region at δ −62.5 are assigned to other products (see text). In the NH_3 region the peaks 2b and 4a are assumed to be concealed by peaks 1 and 3a, respectively (see Table 1).

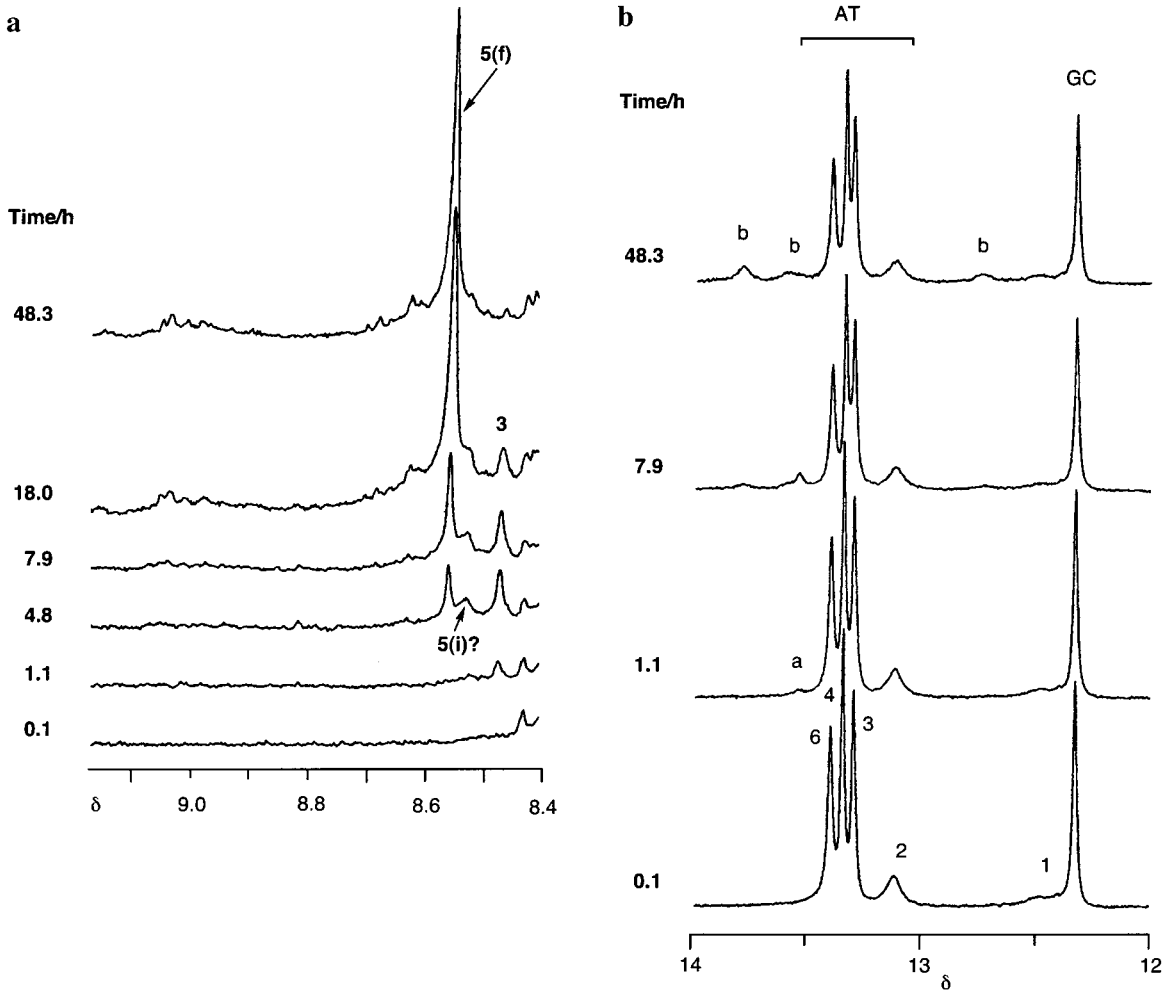

Figure 2. ^{1}H NMR spectra (600 MHz) of (a) the aromatic region and (b) the imino region of duplex **I** after reaction with ^{15}N-**1** for between 0 and 48 h. In (**a**), the peaks are assigned to the H8 resonances of the G5 and G5′ bases coordinated to platinum in the monofunctional adduct (**3**) and the 1,4-interstrand cross-link (**5**). In (**b**), assignments of resonances to base pairs are indicated by numbers (5 = G(5)-C(8*) etc.), and letters indicate assignments to platinated adducts: a, **3** and b, **5**. Although the reaction is complete at 48 h intense signals for unplatinated **I** are present due to the excess of DNA used in the reaction.[23]

and the monoaqua monochloro species (**2**) by [^{1}H,^{15}N] NMR have been reported in detail elsewhere.[22] HPLC purification of ^{15}N-**1** indicated that the purity was >95% but the presence of minor impurities was evident in the [^{1}H,^{15}N] NMR spectrum.[22] Careful analysis of the [^{1}H,^{15}N] NMR spectra showed that these impurity species do not react with DNA (other than through electrostatic interactions) and thus do not contribute to the observed product species. None of the impurity ^{1}H/^{15}N peaks overlapped with the peaks for species **1**−**5** (Figure 1) and therefore their presence in the sample of ^{15}N-**1** did not compromise this kinetic study. A full description of the behavior of the impurity species is provided as Supporting Information.

Platination of DNA. The platination of the self-complementary 12-mer duplex 5′-{d(ATATGTACATAT)$_2$} by ^{15}N-**1** was followed by [^{1}H,^{15}N] NMR by monitoring the time-dependent changes in both the $^{15}NH_3$ and $^{15}NH_2$ regions. Representative spectra of the two regions at different times during the reaction are shown in Figure 1. ^{1}H NMR spectra were also acquired to monitor oligonucleotide base-pairing through examination of the imino resonances (δ = 12−14 ppm) and to verify Pt binding to GN7 by means of the shift of the guanine H8 resonance from that of the unplatinated duplex (δ 7.79). Representative ^{1}H spectra are shown in Figure 2.

Since ^{15}N shifts in Pt am(m)ine species are sensitive to the nature of the trans ligand,[20,21] it was expected that the $^{15}NH_2$ region of the [^{1}H,^{15}N] NMR spectra would be more readily assignable and could be used to follow formation of the different adducts. However, there was considerable overlap of peaks in this region and the sharper $^{15}NH_3$ peaks proved to be more useful. Although these peaks all fell within a narrow region in the ^{15}N dimension (δ −60 to −64) they were well separated in the ^{1}H dimension. It was possible to identify Pt-NH_3 peaks for all species involved in the reaction, largely on the basis of their appearance and disappearance and rationalization of the ^{1}H chemical shifts with reference to the different Pt-NH_3 environments found in molecular models. Careful comparison of the time dependence of the $^{15}NH_3$ and $^{15}NH_2$ regions of the [^{1}H,^{15}N] spectra then allowed identification of nonequivalent NH_2 protons in the monofunctional adduct (**3**), and different conformers of the bifunctional 1,4 interstrand adduct (**5**).

A pH of 5.4 was chosen based on the pH titration curves of the aquated species[22] which indicated that at this pH the Pt-NH_3 peak of the monoaqua monochloro form **2** would appear in a clear region of the spectrum (δ ^{1}H/^{15}N 4.00/−62.6) allowing the concentration of this species to be monitored. Also, this pH lies 0.2 pH units below the pK_a value of **2** (5.62),[22] allowing a more meaningful comparison with previous studies of DNA platination reactions of cisplatin[15,17] which were carried out at pH 6.0 (pK_a of *cis*-[PtCl(NH_3)$_2$(H_2O)]$^{+}$ is 6.41[31]). Likewise,

Table 1. ^{1}H and ^{15}N Shifts for Intermediates Observed during the Reaction of **1** with the Self-Complementary Duplex 5′-{(ATAT**G**TACATAT)$_2$} (pH 5.4)[a]

species 1,1,t,t ($n = 6$)	label	Pt−NH$_3$		Pt−NH$_2$	
		δ ^{1}H	δ ^{15}N	δ ^{1}H	δ ^{15}N (trans ligand)
Y, Y′ = Cl	**1**	3.91	−64.3	5.05	−47.0 (Cl)
		(3.86)	(−64.6)	(5.03)	(−47.0)
Y = Cl, Y′ = OH$_2$	**2**	*b*	*b*	*b*	*b* (Cl)
		4.21	−61.9	*c*	*c* (OH$_2$)
		(4.00)	(−62.6)		
Y = N7G, Y′ = Cl	**3**	3.93	−64.3	5.07, 5.11[d]	−47.0 (Cl)
		4.29	−60.8	5.12	−47.0 (N7G)
Y = N7G, Y′ = OH$_2$	**4**	4.22	−61.9	*e*	*e* (OH$_2$)
		f	*f*	*f*	*f* (N7G)
Y = N7G, Y′ = N7G	**5(i)**	4.32	−61.0	5.11	−47.5 (N7G)
		4.39	−60.5		

[a] ^{1}H referenced to TSP, ^{15}N referenced to ^{15}NH$_4$Cl (external), δ in ^{15}N dimension ± 0.2 ppm. ^{1}H and ^{15}N shifts for **1** and **2** in 15 mM phosphate buffer at pH 5.4 in the absence of DNA are shown in parentheses. [b] Assumed to be concealed by peaks for **1**. [c] NH$_2$ peak for **2** is expected at δ 4.88/−62.2 at pH 5.4;[22] this is too close to H$_2$O to resolve at this concentration (ca. 40 μM). [d] The two NH$_2$ protons are clearly inequivalent but ^{1}H shifts are ± 0.02 ppm due to overlap with **1**. [e] Assumed to lie too close to ^{1}H$_2$O to be visible. [f] Assumed to be concealed by peaks for **3**.

the reactions were carried out at 298 K to allow comparison with those studies of cisplatin.

Chemical considerations allow us to predict that the stepwise formation of an interstrand DNA cross-link will involve, by analogy with the much studied cisplatin,[14,15,17] initial electrostatic binding and aquation, monofunctional binding by covalent attachment of one end to DNA, followed by fixation through bifunctional closure (Scheme 1). Evidence for all of these steps is observed in the current experiments.

Electrostatic Binding and Aquation. The first [^{1}H,^{15}N] spectrum was recorded an average of 14 min after the start of the reaction. In the presence of DNA, both the ^{1}H and ^{15}N shifts of ^{15}N-**1** are slightly deshielded (Pt-NH$_3$ $\Delta\delta$ ^{1}H 0.05, ^{15}N 0.3; Pt-NH$_2$ $\Delta\delta$ ^{1}H 0.02) when compared to a spectrum of a similar control solution of ^{15}N-**1** in the same phosphate buffer at the same pH (Table 1). A peak assigned to the {PtN$_3$O} group of the previously observed monoaqua monochloro species **2** is observed in the NH$_3$ region at δ 4.21/−61.9. When compared to the predicted values for pH 5.4, the $\Delta\delta$ values for the Pt-NH$_3$ group of **2** (0.21 (^{1}H) and 0.7 (^{15}N)) are greater than those seen for **1** (Table 1). Species **2** accounts for 2.5% of the Pt-NH$_3$ species after 14 min, which is slightly less than observed for the control solution in the absence of DNA (5% after 10 min). The peak for **2** is visible in the [^{1}H,^{15}N] spectra until ca. 15 h have elapsed. At pH 5.4 the ^{1}H,^{15}N peak for the Pt-^{15}NH$_2$ group of **2** (δ 4.88/−62.2)[22] lies too close to the ^{1}H$_2$O peak to be observed at this low concentration (ca. 40 μM).

The Monofunctional Binding Step. The concentration of **1** decreases to 50% in ca. 5 h which is significantly shorter than the half-life of 10.5 h observed for reaction of cisplatin at the GpG site of a 14-mer duplex under similar conditions (298 K, pH 6).[15] Two ^{1}H,^{15}N peaks assignable to nonequivalent Pt-^{15}NH$_3$ environments in the monofunctional G/Cl adduct (**3**) were first observable after ca. 15 min. One peak (δ 4.29/−60.8, labeled **3a** in Figure 1) has a ^{1}H shift that is strongly deshielded (by 0.38 ppm) compared to the ^{1}H shift of **1** and is assigned to the Pt-(NH$_3$)$_2$ group coordinated to the guanine N7 of **I**. The second peak (δ 3.93/−64.3, **3b**) lies very close to the Pt-NH$_3$ peak for **1** and is reasonably assigned to the uncoordinated Pt-(NH$_3$)$_2$ group. The two sets of Pt-^{15}NH$_3$ peaks attributed to the monofunctional adduct have comparable intensities until ca. 11 h when the relative intensity of peak **3a** increases as a result of overlap with peaks from the 1,4 GG interstrand adduct. Nevertheless, we were able to obtain reliable concentrations for the monofunctional adduct from the second peak (**3b**), which is observed free from overlap throughout the entire course of the reaction (Figure 1). The monofunctional adduct reaches a maximum concentration of ca. 40% of the total platinum after ca. 8 h and then decreases.

Assignment of the ^{1}H,^{15}N peaks for the Pt-^{15}NH$_2$ groups of the monofunctional adduct (**3**) was more complicated due to overlap in this region. Based on previous work with cisplatin[14,15,17] we expected that coordination of the platinum to the duplex GN7 would result in significant shifts in both ^{1}H and ^{15}N dimensions for the trans ^{15}NH$_2$ group. The uncoordinated Pt-^{15}NH$_2$ group would be expected to give a peak overlapped with, or slightly deshielded with respect to, **1** (as for the Pt-^{15}NH$_3$ group). One broad peak with a time-dependent profile consistent with **3** was observed at δ 5.12/−47.0. The ^{15}N shift is identical to **1** and the ^{1}H shift is deshielded by only 0.07 ppm. Comparison of time-dependent changes in the peak volumes in the ^{15}NH$_2$ and ^{15}NH$_3$ regions indicated that the peak at δ 5.12/−47.0 must have a contribution from the two protons (X_1, X_2) of the guanine-N7 coordinated Pt-NH$_2$ group and one proton (Y_1) of the unbound Pt-NH$_2$ group. The resonance of the other proton (Y_2) is overlapped with the peak for **1**. This suggests that the two Pt-NH$_2$ groups have similar environments and the Pt-NH$_2$ group coordinated trans to the duplex does not interact strongly with the DNA. The identical ^{15}N shifts for **1** and both Pt-NH$_2$ groups of **3** is surprising but the resolution in the ^{15}N-dimension is relatively poor (δ ±0.2 ppm).

In the aromatic region of the ^{1}H spectrum (Figure 2a) a peak at δ 8.50 is assignable to the H8 of the coordinated G residue of **3**, based on its time-dependent profile, which is similar to that observed for **3** in the [^{1}H,^{15}N] spectra. In the imino region (Figure 2b), there is one shifted resonance at δ 13.54 assignable to an AT base pair in **3**.

The Bifunctional Adduct. Fixation of the Interstrand Cross-link. Closure of the monofunctional adduct (**3**) is complete 48 h after commencing the reaction. Closure of **3** to form the 1,4 GG interstrand cross-link (**5**) could occur directly and/or involve prior aquation of **3** to form a G/H$_2$O intermediate (**4**). Evidence for the latter is provided by the appearance after ca. 2.5 h of a small peak (δ 4.22/−61.9) in the Pt-NH$_3$ region of the [^{1}H,^{15}N] NMR spectrum (labeled **4b** in Figure 1). The peak remains relatively constant at 0.2% of the total platinum until 12 h, then it decreases and is no longer observed after 18 h. Assignment of this peak as **4** (G/H$_2$O) is reasonable based on the ^{1}H/^{15}N chemical shift which is very close to the peak for the {PtN$_3$O} group of the monoaqua monochloro species (**2**). The ^{15}N shifts are identical and the ^{1}H shift is deshielded by 0.01 ppm. The deshielding of the ^{1}H shift of the Pt-NH$_3$ groups of the unbound {PtN$_3$O} end of **4** in comparison to **2** is therefore similar to those noted above for the (unbound) {PtN$_3$-Cl} group in **3** (G/Cl) in comparison to **1**. The ^{1}H/^{15}N shifts of the ^{15}NH$_2$ peak for the uncoordinated {PtN$_3$O} group in **4** would be expected to be similar to that of **2**, and not resolved in these spectra because of the proximity to the ^{1}H$_2$O resonance.

^{1}H,^{15}N peaks assignable to the 1,4-interstrand GG adduct (**5**) are first visible after ca. 1 h. The spectrum recorded after 2.1 h is shown in Figure 1a. At this point the spectrum can be

(30) Orozco, M.; Laughton, C. A.; Herzyk, P.; Neidle, S. *J. Biomol. Struct. Dyn.* **1990**, *8*, 359−373.

(31) Berners-Price, S. J.; Frenkiel, T. A.; Frey, U.; Ranford, J. D.; Sadler, P. J. *J. Chem. Soc., Chem. Commun.* **1992**, 789−791.

interpreted as formation of a single initial conformation (or possibly a combination of very similar conformations) of the 1,4 GG adduct **5** (termed **5(i)**). In the $^{15}NH_3$ region the first set of peaks assignable to the bifunctional adduct is a broadened shoulder at δ 4.32/−61.0, slightly deshielded from the monofunctional G/Cl peak (**3a**), and a sharper more strongly deshielded peak at δ 4.39/−60.5. The presence of independent peaks of equal intensity indicates two distinct environments for the four Pt-NH_3 groups. From consideration of the molecular model of the 1,4-interstrand cross-link on B-form DNA (Figure 5) and the behavior of these two peaks over time (see below and Figure 1), we assign the sharp peak at δ 4.39/−60.5 to the Pt-NH_3 environments B_1 and B_2 which are both hydrogen bonded to a guanine O6. The broader peak slightly downfield of **3a** is assigned to the Pt-NH_3 A_1 and A_2 groups which the model shows are in more varied environments pointing toward the phosphate backbone:

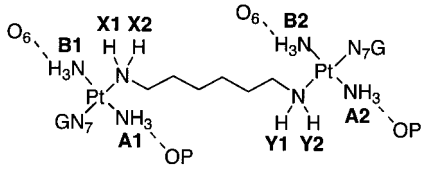

In the $^{15}NH_2$ region, initially only a single broadened peak is visible at δ 5.11/−47.5 (Figure 1a), which indicates that **5(i)** has identical ^{15}N shifts for the two NH_2 groups as well as similar ^1H shifts for all 4 NH protons (i.e., δ $X_1 \approx X_2 \approx Y_1 \approx Y_2$). These ^1H shifts are almost identical with those of the monofunctional adduct (**3**,**G/Cl**) and the ^{15}N shift is also very similar ($\Delta\delta$ 0.5). As noted above our data indicate that the monofunctional adduct (**3**) already has three NH_2 protons in similar environments (δ $X_1 \approx X_2 \approx Y_1 \neq Y_2$) and these data suggest that macrochelate ring closure to form **5(i)** brings the fourth NH_2 proton into a similar environment.

Conformational Flexibility of the 1,4-Interstrand Cross-link. Evidence for the presence of conformers of **5** was obtained from observation of the time-dependent changes in the [^1H,^{15}N] spectra and in particular the appearance of several new $^1H/^{15}N$ peaks in the NH_2 region (Figure 1). Sequential changes are observed culminating in the irreversible formation of final product conformer(s) **5(f)**. The interconversion between **5(i)** and **5(f)** and the effect of temperature on the distribution of **5(f)** conformers at equilibrium is the subject of a separate study to be published elsewhere.[32]

Briefly, in the NH_3 region the peak at δ 4.39/−60.5 (assigned to the O6 H-bonded B_1 and B_2 groups in **5(i)**) remains relatively sharp and steadily increases in intensity until the reaction is complete. Throughout the course of the reaction the volume of this peak (and the shoulder to high frequency that becomes visible at later time points) consistently accounts for ca. 50% of the total $^1H/^{15}N$ peaks derived from the mixture of **5** conformers. On the other hand, new environments for the A_1 and A_2 NH_3 groups in **5(f)** are indicated by the appearance of new peaks, as shown in Figure 1. The $^{15}NH_2$ region of the [^1H,^{15}N] spectrum at the end of the reaction (49 h, Figure 1) shows that the peaks for the bifunctional adduct product conformers **5(f)** are concentrated at three distinct ^{15}N shifts, δ −48.4, −47.5, and −45.6. For the latter peak, in particular, there is evidence for overlap of peaks at slightly different ^{15}N chemical shifts. The two peaks at −48.4 ppm (δ ^1H ca. 5.23 and 5.13) have a similar line shape and intensity and account for ca. 46% of the total **5(f)** adduct(s). The peaks centered at ^{15}N δ −47.5 (ca. 22%) and −45.5 (ca. 31%) appear as single merged peaks covering a wide chemical shift range in the ^1H dimension.

Evidence that the different peaks in the [^1H,^{15}N] NMR spectrum correspond to different conformers of the 1,4-interstrand cross-link is provided by the aromatic region of the ^1H spectrum where there is only one major peak (at δ 8.59) assignable to the GH8 protons of the final adduct **5(f)** (Figure 2a). A small peak at δ 8.56 may be attributable to **5(i)** as it is first visible after ca. 1 h but does not persist in the final product (Figure 2a). In the imino region (Figure 2b) there are two downfield shifted resonances (δ 13.79 and 13.59) assignable to AT base pairs in the bifunctional adduct. A new peak at δ 12.75 is assignable to GH1, which is expected to be shifted slightly downfield upon platination.[33] These peaks appeared between 1 and 5 h from the start of the reaction.

HPLC characterization of the final product was carried out by repeating the reaction under identical conditions to the NMR experiments. The HPLC elution profile of the final product (see Supporting Information) showed one major product peak with minor peaks accounting for only 7% of the total product, consistent with the NMR data (see below). The major peak was separated and characterized by ESI mass spectroscopy. The results (see Supporting Information) are consistent with a cross-linked adduct of **1** and duplex **I**.

Kinetic Analysis. For the purposes of the kinetic fit the volume of all ^1H,^{15}N peaks assignable to the Pt-NH_3 groups of the bifunctional adduct conformers were summed for each time point. Although the A_1/A_2 and B_1/B_2 NH_3 peaks of the **5(f)** conformers cover a wide range of ^1H shifts, the peaks are concentrated in a relatively narrow band of ^{15}N shifts centered at ca. 60.5 ppm (Figure 1d). The notable exceptions are the few peaks with ^{15}N shifts at ca. −62.5 ppm which represent ca. 6% of the final product. Peaks in this region are first detected after ca. 2.5 h but they increase only slowly (e.g., <2% after 9 h, Figure 1c). The relative intensity and time-dependent profiles of the peaks are similar to those of a cluster of peaks that appear in the H8 region of the ^1H spectra between 9.0 and 9.1 ppm and are assigned to other (cross-linked) adducts formed from **3**. The volumes of peaks at ^{15}N δ −62.5 were summed and included in the kinetic model as other products (Scheme 1). The time dependencies of the concentration of species in the reaction are shown in Figure 3.The kinetic data were fitted to a number of models. The pre-covalent binding association of **1** and **2** with the duplex was not considered and both species were treated as unbound. The aquation of **1** is rapid and the equilibrium established lies strongly in favor of the dichloro form.[22] The formation of the diaquated species from **2**, assumed to occur in the same ratio as formation of **2** from **1**, is a very minor contributor at equilibrium and was therefore not included in the kinetic model for the binding of **1** to DNA. Models in which reversible aquation was allowed using the rate constants derived from Cl^- release experiments[22] proved unsuccessful but were based on data obtained at 310 K (rather than 298 K). The anation rate constant was fixed and the aquation (forward) rate constant was allowed to vary to fit the curve. In all cases good fits could be obtained for **1** and the monofunctional adduct (**3**), at the expense of the fit of the monoaqua monochloro species (**2**). As a result an irreversible aquation process was assumed. The monofunctional adduct (**3**) was assumed to come solely from **2** and direct binding of **1** to the DNA was not considered.

(32) Berners-Price, S. J.; Cox, J. W.; Davies, M. S.; Qu, Y.; Farrell, N. Manuscript in preparation.

(33) Qu, Y.; Scarsdale, J. N.; Cox, J.; Farrell, N.; De Cillis, G. *8th International Symposium on Platinum and other Metal Coordination Compounds in Cancer Chemotherapy*: Oxford, UK, March, 1999; Abstract 4.O6.

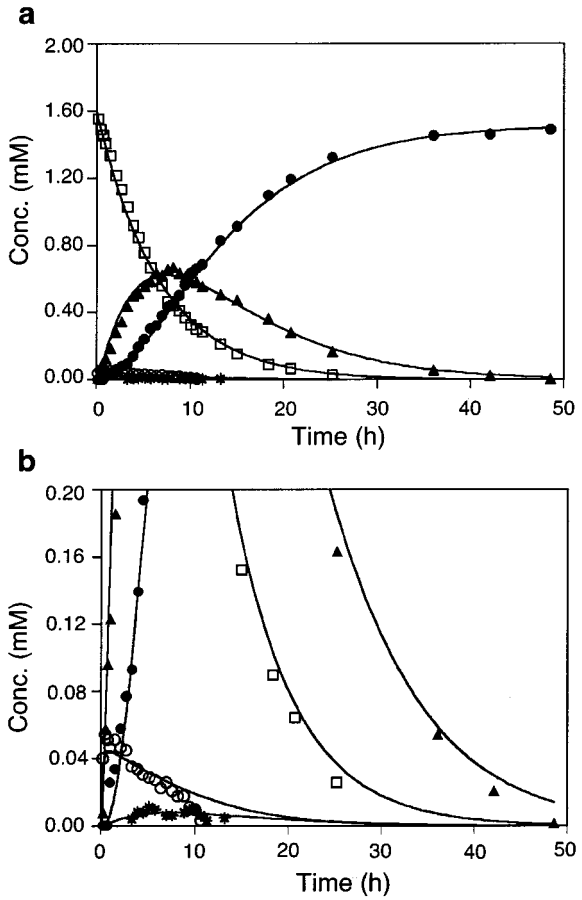

Figure 3. Plot of the relative concentration of species observed during the reaction at 298 K between **I** and ^{15}N-**1** (Scheme 1). The curves are computer best fits for the rate constants shown in Table 2 (labels: square, **1**; open circle, **2**; triangle, **3**; asterisk, **4**; solid circle, **5**). The concentrations are based on the relative peak volumes of peaks in the Pt−NH_3 region.

Practical limitations (such as quantities of reagents for titrations at different ^{15}N-**1**:**I** ratios and the spectrometer time involved) preclude separation of the contributions of the direct and indirect (via the aquated species) kinetic routes. The reaction of **2** with the duplex to form **3** was an irreversible second-order process overall: first order with respect to both the concentration of **2** and duplex. The monofunctional adduct (**3**) was either treated as ring closing directly to the bifunctional 1,4-interstrand GG adduct (**5**) or first aquating to form a monofunctional aqua species (**4**) which then ring closes to form **5**. Both processes were treated as irreversible first order with respect to the concentration of **3** or **4**. The rate constants obtained from the two kinetic models are listed in Table 2 and the computer best fits for the rate constants are shown in Figure 3.

Molecular Models. (a) Monofunctional Adduct. The model for the monofunctional (G/Cl) adduct **3** is shown in Figure 4. An NH_3−O6 hydrogen bond is observed between an ammine hydrogen on the Pt-$(NH_3)_2$ unit coordinated to the N7 atom of G5* and the O6 of that guanine (H−O6 distance = 1.9 Å). No helical distortion is necessary for the formation of this hydrogen bond. However, the Pt coordination sphere (PtN_3 plane) is not restricted by bifunctional binding (as for cisplatin), and forms a dihedral angle of ∼40° with the plane of G5*. This places the other ammine group toward the region of the phosphate backbone and allows the formation of a hydrogen bond with a phosphate oxygen (distance = 2.0 Å). The monofunctional binding of the platinum complex induces partial disruption of the base pairing at the binding site (G5*−C8′) and its adjacent base pair (T4−A9′) as determined by comparison of propeller twist values (see Supporting Information).[34,35] The unbound end of **3** interacts with the phosphate backbone of duplex **I** by an electrostatic attraction between the positively charged Pt coordination sphere and the negatively charged DNA. Specifically, hydrogen bonds are observed between a proton from each ammine group and the phosphate backbone (distances = 1.8 Å). There are no hydrogen bonds observed involving any of the four amine protons.

Table 2. Rate Constants for the Overall Reaction of **1** with the Self-Complementary Duplex 5′-{(ATAT**G**TACATAT)$_2$} at 298 K (pH 5.4)[a]

rate constant	including G/H_2O (**4**)	no G/H_2O
$k_H/10^{-5}$ s^{-1}	4.15 ± 0.04	4.15 ± 0.04
k_{MF}/M^{-1} s^{-1}	0.47 ± 0.07	0.47 ± 0.06
$k_{MH}/10^{-5}$ s^{-1}	3.62 ± 0.04	
$k_{CH}/10^{-5}$s^{-1}		3.39 ± 0.04
k_{BF}/s^{-1}	0.0027 ± 0.0015	
$k_{BFO}/10^{-5}$ s^{-1}	15.6 ± 9.2	

[a] The reactions were modeled as going through the G/H_2O species (**4**) prior to closure of the bifunctional adduct (Scheme 1), and were also modeled without the G/H_2O intermediate. The errors represent one standard deviation.

(b) Bifunctional Adduct. The model for the bifunctional adduct in B-form DNA is shown in Figure 5. The flexibility and length of the linker group do not force the helix to bend to accommodate formation of a bifunctional adduct. Therefore, helical distortion is minimal and localized near the binding sites. The DNA is not significantly kinked, in agreement with bending studies on site-specific adducts formed in similar sequences,[9] and base pairing is mostly maintained (see Figure 5b). The binding of **1** at G5* and G5′* slightly disrupts the base pairing T4−A9′ and A9−T4′. The propeller twist values for these base pairs are more positive (ca. −9.3°) than for the rest of the sequence (ca. −12.3°). The helix is also wound slightly tighter in this region in comparison to canonical DNA (see twist and roll in the Supporting Information).[34,35]

The two guanine-N7-bound ends of the bifunctional adduct exhibit interactions similar to those for the bound Pt end of the monofunctional model above. One NH_3 group on each Pt coordination sphere (B_1 and B_2, Figure 5) hydrogen bonds to O6 of the bound guanine (distances = 1.9 Å). The other two Pt-NH_3 groups (A_1 and A_2, Figure 5) point toward the phosphate backbone. An ammine proton (A_1) exhibits a slightly weaker hydrogen bond (relative to those to O6) to an oxygen of the phosphate backbone (distance = 1.9 Å). The other ammine proton (A_2) does not show hydrogen bonding to **I**, although due to the rotational flexibility of the ammine and the overall flexibility of the backbone, a weak or solvent-mediated interaction between A_2 protons and a phosphate oxygen of G5′* cannot be ruled out. There are no hydrogen bonds observed involving the amine protons.

Discussion

Kinetics and Mechanism of Formation of the 1,4-Interstrand Cross-link. The use of [^{1}H,^{15}N] HSQC NMR combined with molecular modeling data has allowed us to develop a detailed picture of the mechanism of formation of a long-range

(34) Dickerson, R. E.; Bansal, M.; Calladine, C. R.; Biekmann, S.; Hunter, W. N.; Kennard, O.; Lavery, R.; Nelson, H. C.; Olson, W. K.; Saenger, W.; Shakked, Z.; Sklenar, H.; Soumpasis, D. M.; Tung, C. S.; Wang, A. H. C.; Zurkin, V. B. *EMBO J.* **1989**, 1−4.
(35) Dornberger, U.; Flemming, J.; Fritzsche, H. *J. Mol. Biol.* **1998**, *284*, 1453−1463.

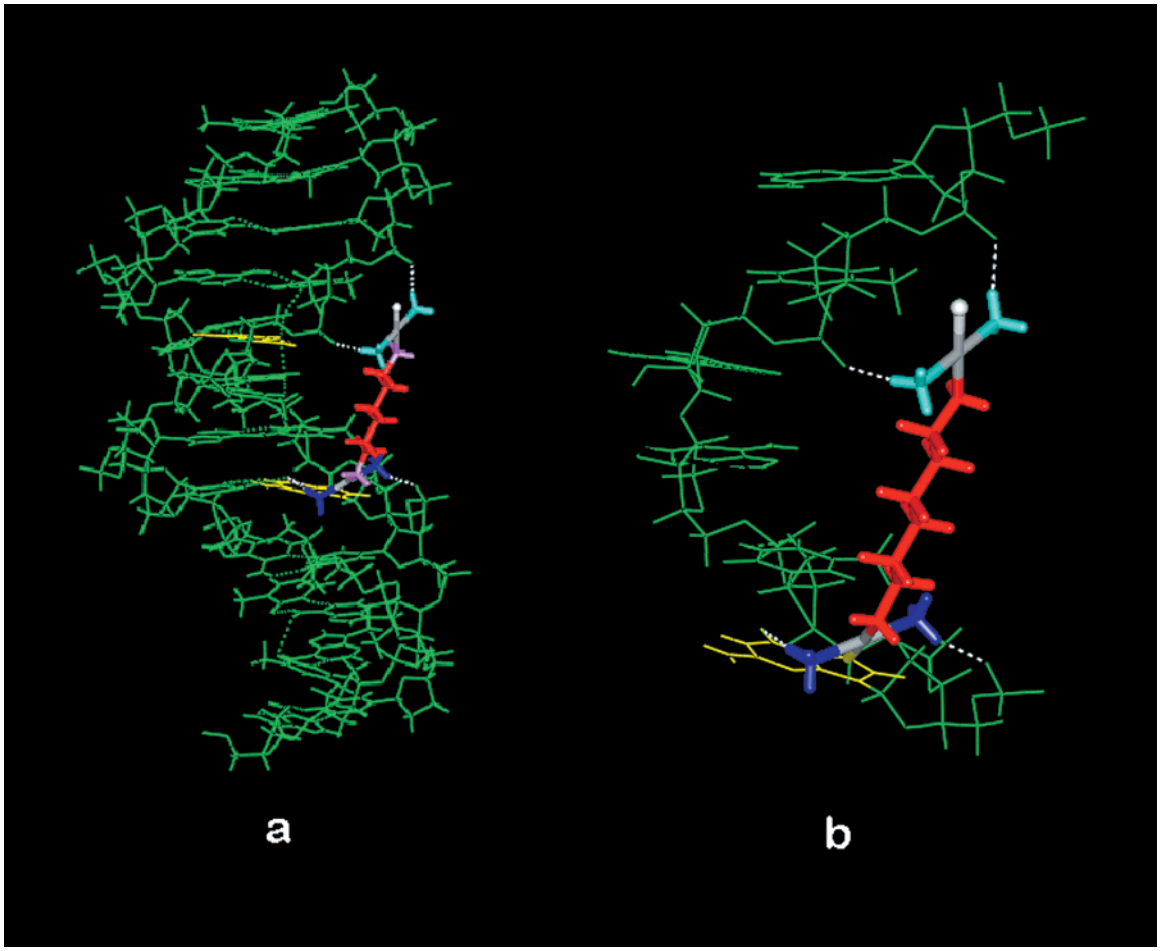

Figure 4. (a) Molecular model of the monofunctional adduct (**3**) formed by **1** and duplex **I**; (b) close up of hydrogen bonding between the Pt-NH_3 groups and the duplex (in white); bases not involved in the interaction are omitted for clarity: **I** (green), guanine G5* and G5′ (yellow), $-(CH_2)_6-$ linker of **1** (red), NH_3 groups of unbound end (light blue), NH_3 groups of bound end (blue), NH_2 groups (pink).

1,4-interstrand cross-link by the dinuclear platinum complex **1**. The first step is an electrostatic interaction of **1** with the DNA surface, as evidenced by the slight deshielding of the ^{1}H shifts of the Pt-NH_3 and Pt-NH_2 protons (Table 1). This observation of preassociation, not previously noted in the cisplatin case,[14,15,17] is likely through electrostatic and hydrogen-bonding interactions as a consequence of the higher charge of the dinuclear species. The stronger deshielding of **2** compared to **1** reflects the higher charge of the {PtN_3O} group and hence a stronger (electrostatic) interaction with the DNA. In agreement with this, similar preassociation is observed for the interaction of the clinical drug 1,0,1/t,t,t (carrying a 4+ charge) with the same sequence.[36] Recent evidence for noncovalent binding association of cationic dinuclear platinum antitumor complexes has been obtained from a ^{1}H NMR study of the oligonucleotide binding of the dinuclear platinum complex [(en)Pt(μ-dpzm)$_2$Pt(en)]$^{4+}$ to the dodecanucleotides d(CGCGAATTCGCG)$_2$ and d(CAATCCGGATTG)$_2$.[37]

The rate-limiting step in the binding of cisplatin to DNA has long been considered to be aquation of the first chloro ligand,[38] and prior to this present study it was not clear whether this was also the case for di- and trinuclear antitumor complexes.[8,39] Our results now show that the monoaqua monochloro species (**2**) is formed prior to any covalent binding to DNA and that aquation is the rate-limiting step in formation of the monofunctional adduct. The aquation pseudo-first-order rate constant is lower than the value of 8.5×10^{-5} s^{-1} obtained for **1** in the absence of DNA and at a higher temperature (310 K),[22] but in the present case the aquation reaction was modeled as irreversible. The aquation rate constant of **1** is ca. 4-fold higher than the reported aquation rate constants for cisplatin ($(1.1 \text{ to } 1.8) \times 10^{-5}$ s^{-1}) prior to monofunctional binding to 14-mer duplexes containing GpG, ApG, and GpA sites, under similar conditions (298 K, pH 6.0) and where the aquation step was also modeled as an irreversible reaction.[15,17]

It is interesting to note that the aquation of **1** appears to be slowed in the presence of DNA. A similar slowing of cisplatin aquation has been observed, and attributed to a possible association between cisplatin and DNA that limits solvent access to the Pt.[40] Likewise, in the present case, the slowing could occur following the observed electrostatic interaction between the dipositive **1** and the polyanionic DNA. Such electrostatic interactions could produce subtle variations in the aquation sphere of the platinum centers required to produce the five-membered transition state necessary for substitution (aquation) reactions.

The rate constant for monofunctional binding of **2** to duplex **I** (TpGpT sequence) may be compared to that of the mono-

(36) Hegmans, A.; Cox, J. W.; Berners-Price, S. J.; Guo, Z.; Qu, Y.; Davies, M. S.; Farrell, N. Manuscript in preparation.
(37) White, N. J.; Collins, J. G. *J. Inorg. Biochem.* **2000**, *78*, 313−320.
(38) Johnson, N. P.; Hoeschele, J. D.; Rahn, R. O. *Chem.-Biol. Interact.* **1980**, *30*, 151−169.
(39) Kloster, M. B.; Hannis, J. C.; Muddiman, D. C.; Farrell, N. *Biochemistry* **1999**, *38*, 14731−14737.
(40) Davies, M. S.; Berners-Price, S. J.; Hambley, T. W. *Inorg. Chem.* **2000**, *39*, 5603−5613.

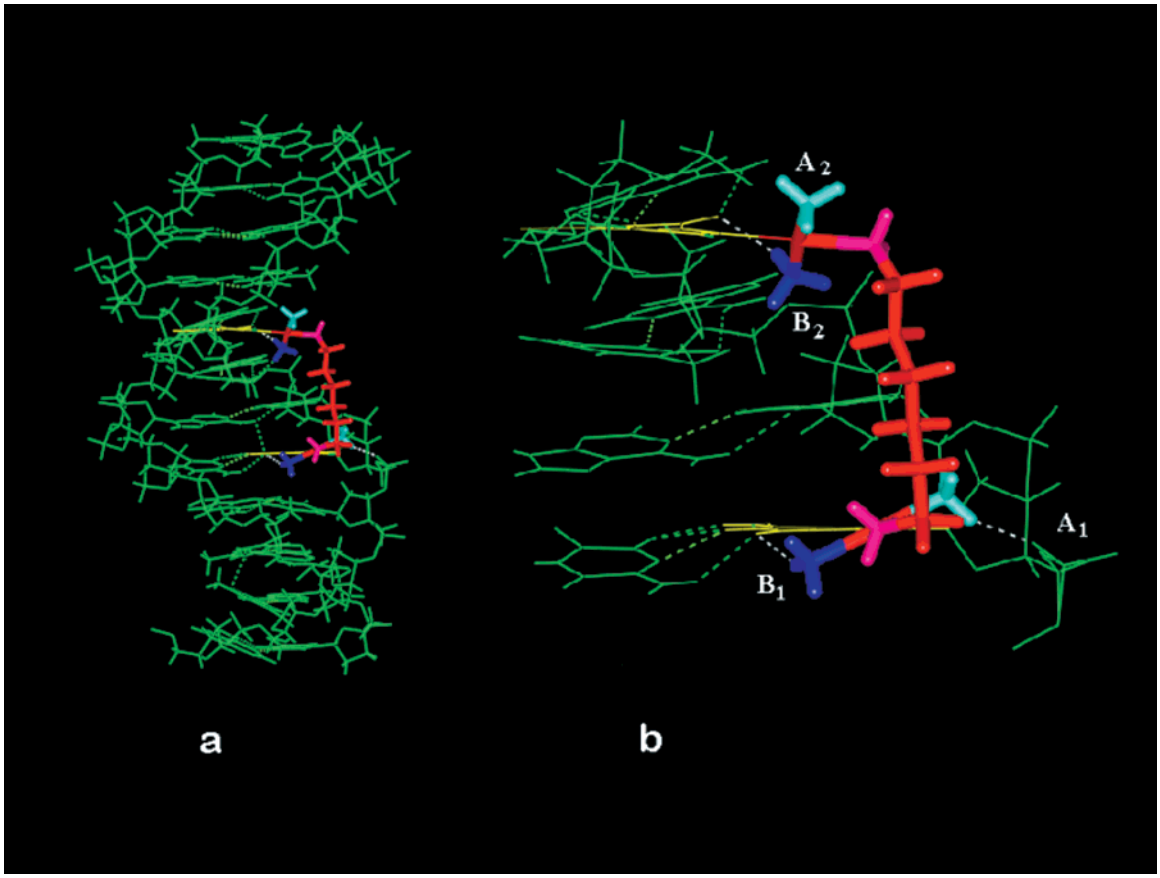

Figure 5. (a) Molecular model of the bifunctional 1,4 interstrand cross-link formed by **1** and duplex **I** (B-form DNA, corresponds to **5(i)**); (b) close up of hydrogen bonding between the Pt-NH_3 groups and the duplex (in white); bases not involved in the interaction are omitted for clarity: **I** (green), guanine G5* and G5′ (yellow), $-(CH_2)_6-$ linker of (**1**) (red), NH_3 groups H-bound to O6 (dark blue), NH_3 groups toward backbone (light blue), NH_2 groups (pink).

functional binding of *cis*-$[PtCl(NH_3)_2(H_2O)]^+$ to the isolated guanine N7 of a TpGpA sequence in duplex DNA which was ca. 25-fold lower (0.023 M^{-1} s^{-1}).[17] Interestingly, the rate constant for monofunctional adduct formation observed here is comparable to that of *cis*-$[PtCl(NH_3)_2(H_2O)]^+$ binding to the 3′ and 5′ G of a 14-mer duplex containing a GpG site (0.47 and 0.15 M^{-1} s^{-1} respectively).[15]

The results presented herein provide evidence that aquation of the monofunctional (G/Cl) adduct to form a G/H_2O intermediate occurs prior to closure to form the bifunctional 1,4-interstrand cross-link and that the aquation is the rate-limiting step in this process (Table 2). However, the ^1H,^{15}N peak for the G/H_2O species (**4**) is of very low intensity and the assignment (although plausible) is unconfirmed. A G/H_2O peak could also occur as a result of direct reaction of the diaquated form of **1** with the duplex. However, given the assumption that the two {PtN_3Cl} groups of **1** act independently of one another and therefore the equilibrium constant for the second aquation step will be similar to that of the first,[22] it is unlikely that any products of the reaction of the diaqua species with **I** will be present at detectable concentrations.

The kinetics for bifunctional adduct fixation were modeled with and without inclusion of the G/H_2O intermediate. The low concentration of the G/H_2O species results in larger fitting errors for the closure step from **4** to **5** than are obtained from the direct closure model. The direct rate constant for closure (k_{CH}) encompasses the aquation of the monofunctional chloro adduct as well as the closure of the monofunctional aqua adduct into one first-order process. The rate constant for direct closure from the G/Cl adduct is slightly lower than the rate constant for aquation of G/Cl (k_{MH}), indicating that aquation is rate limiting. The rate constant for closure of the G/H_2O species (k_{BF}), however, is very high; this has the effect of preventing the accumulation of the G/H_2O adduct in solution to more than trace levels.

Overall, bifunctional adduct formation is ca. 10−55-fold faster than closure of 5′ and 3′G monofunctional adducts generated by the diaqua form of cisplatin (at 288 K).[16] However, the mechanisms of bifunctional adduct formation are distinctly different in the two cases. For cisplatin macrochelate ring closure involves rotation about one Pt−GN7 bond prior to bond formation with the second (adjacent) nucleoside. For the dinuclear complex, the rate of closure relates to the movement of the unbound Pt grouping, and then binding of this PtN_3O (or PtN_3Cl) to the GN7 on the other strand. The pre-covalent binding association (electrostatic interaction) of the unbound end (of either **3** or **4**) is likely to contribute to the fast fixation of the long-range interstrand cross-link.

Structures of the Monofunctional and Bifunctional Adducts. For the monofunctional adduct **3** the NMR data are largely consistent with the hydrogen-bonding interactions observed in the molecular model (Figure 4). The peak at δ 4.29/−60.8 (**3a**, Figure 1) can be assigned to the two ammine groups on the Pt bound to the DNA. The shift to high frequency is indicative of strong hydrogen bonding. The observation of a single (slightly broadened) peak indicates that the two NH_3 groups are in very similar environments. The model is consistent with this interpretation with both ammines forming hydrogen bonds to an oxygen (guanine O6 or phosphate). The ^1H,^{15}N peak for the uncoordinated Pt-$(NH_3)_2$ group of **3** (**3b**, Figure 1)

is deshielded slightly ($\delta\Delta$ 0.02) with respect to **1** indicative of an electrostatic attraction between the positively charged Pt coordination sphere and the negatively charged DNA. This interaction is also seen in the model where there are hydrogen bonds between the ammine groups and the phosphate backbone. There are no hydrogen bonds involving any of the four amine protons of the monofunctional adduct and this is consistent with the NMR results which show similar $^1H/^{15}N$ shifts for the NH_2 protons of **3** and **1**. The ^1H NMR spectrum of **3** shows a downfield shifted imino resonance at δ 13.54, also consistent with the model that shows partial disruption of the base pair (T4−A9′) adjacent to the binding site.

For the bifunctional adduct the models must take into account the presence of observed conformers. An intriguing possibility is that the alternating purine−pyrimidine sequence used here may undergo a B → Z conformational change, as demonstrated previously for poly(dG-dC)·poly(dG-dC), upon bifunctional adduct formation by both dinuclear and trinuclear compounds.[8] The interconversion between the conformers and the effect of temperature on the distribution of **5(f)** conformers at equilibrium is not presented in detail here and will be the subject of a separate study to be published elsewhere.[32] For these reasons we chose as a reasonable starting point in this paper to model the bifunctional adduct only as initially formed in B-form DNA.

The model (Figure 5) is largely consistent with the interpretation of the NMR results for the initially formed conformer **5(i)**. The sharp peak at δ 4.39/−60.5 (deshielded 0.48 ppm from **1**) is assignable to the Pt-NH_3 environments B_1 and B_2. These groups are coordinated to different Pt atoms in the binuclear complex and exist in essentially identical environments, strongly hydrogen bonded to the O6 of G5* and G5′*, respectively. The $^1H/^{15}N$ peak assignable to the Pt-NH_3 A_1 and A_2 environments of **5(i)**) is observed as a broadened shoulder slightly downfield of the monofunctional peak **3a** (Figure 1). The model (Figure 5) shows that the A_1/A_2 groups point toward the phosphate backbone and these environments will be similar to those of the coordinated end of the monofunctional adduct (**3**), given that in the latter case free rotation will produce an average of the two environments hydrogen bonded to O atoms. There are no hydrogen bonds involving the amine protons and this corresponds to the equivalency of the NH_2 peaks (δ 5.11/−47.5) in the NMR spectra for **5(i)**.

Interconversion of conformers is accompanied by changes in the NH_2 region of the $[^1H,^{15}N]$ NMR spectrum and a reasonable interpretation is that there are a variety of thermodynamically preferred conformers of the 1,4 GG interstrand cross-link, in which there are several distinct environments for the Pt-NH_2 groups. These environments would be very different to those of the kinetically favored conformer **5(i)** in which the model (Figure 5) shows that the NH_2 protons are positioned away from the DNA and have no contacts with anything other than solvent.

Conclusions

Interstrand cross-linking is a potent and varied lesion which is responsible for the cell-killing effects of many anticancer drugs.[6] The studies reported here elucidate the mechanism of formation of site-specific long-range (1,4)-interstrand cross-links by dinuclear platinum compounds, previously studied by molecular biology techniques.[41]

A major rationale for these studies is the desire to compare the DNA-binding profile of a typical dinuclear platinum anticancer drug with that of cisplatin. In particular, a study of both kinetics and structure may lead to an understanding of how different and distinct DNA−drug binding profiles may be manifested as a unique profile of antitumor activity. Overall, the results show that the higher rate of bifunctional DNA adduct formation by **1**, in comparison to cisplatin, is brought about principally by a higher rate of aquation and more rapid bifunctional fixation of the monofunctional adduct. The NMR analysis confirms the conformational flexibility of the cross-link, a feature expected to contribute to the distinct differences in biological profile between dinuclear and mononuclear platinum anticancer drugs. This flexibility and consequent lack of a directed bend may further contribute to the fact that 1,4-interstrand cross-links are not recognized efficiently by proteins such as HMG1,[10] which recognize rigid, bent DNA such as that induced by cisplatin 1,2-intrastrand adducts.[11,12] Study of structurally related but distinct Pt-DNA adducts may lead to further insight of "downstream" effects initiated through differential protein recognition that may produce unique antitumor effects.[42]

Acknowledgment. This work was supported by the Australian Research Council, National Institutes of Health (RO1-CA78754), National Science Foundation (INT-9805552 and CHE-9615727), and the American Cancer Society (RPG89-002-11-CDD). We thank Dr. Zijian Guo (Nanjing) for helpful discussions and Dr. G. Pierens for assistance with NMR experiments. We also thank Dr. Walter Barklage for the preparation of ^{15}N-**1** and Mr. James C. Hannis and Dr. David C. Muddiman for the mass spectrometry.

Supporting Information Available: SCIENTIST models used to determine the rate constants given in Table 2, HPLC chromatograms of the unpurified and purified final product from the reaction, ESI-FTICR mass spectrum for the duplex [d(ATATGTACATAT)$_2$-[{*trans*-Pt($^{15}NH_3$)$_2$}$_2$(μ-$^{15}NH_2$(CH_2)$_6$$^{15}NH_2$)]], a discussion of the impurity species in the sample of ^{15}N-**1**, methodology for molecular model development and minimization, and a table of molecular modeling DNA base step and base pair parameters for the bifunctional adduct (PDF). This material is available free of charge via the Internet at http://pubs.acs.org.

JA0012772

(41) Zou, Y.; Van Houten, B.; Farrell, N. *Biochemistry* **1994**, *33*, 5404−5410.

(42) Zamble, D.; Lippard, S. J. In *Cisplatin. Chemistry and Biochemistry of a Leading Anticancer Drug*; Lippert, B., Ed.; Wiley VCH: New York, 1999; pp 73−110.